Aliasing, coherence, and resolution in a lensless holographic microscope

Agbana, Tope; Gong, Hai; Amoah, A.S.; Bezzubik, V; Verhaegen, Michel; Vdovin, Gleb

DOI
10.1364/OL.42.002271

Publication date
2017

Document Version
Accepted author manuscript

Published in
Optics Letters

Citation (APA)
Agbana, T., Gong, H., Amoah, A. S., Bezzubik, V., Verhaegen, M., & Vdovin, G. (2017). Aliasing, coherence, and resolution in a lensless holographic microscope. *Optics Letters*, *42*(12), 2271-2274. https://doi.org/10.1364/OL.42.002271

Aliasing, coherence, and resolution in a lensless holographic microscope

TEMITOPE E. AGBANA[1,*], HAI GONG[1], ABENA S.AMOAH[4], VITALY BEZZUBIK[3], MICHEL VERHAEGEN[1], AND GLEB VDOVIN[1,2,3]

[1] Delft University of Technology, DCSC, Mekelweg 2, 2628 CD Delft, The Netherlands
[2] Flexible Optical B.V., Polakweg 10-11, 2288 GG Rijswijk, The Netherlands
[3] ITMO University, Kronverksky 49, 197101 St Petersburg, Russia
[4] Leids Universitair Medisch Centrum,Albinusdreef 2, 2333 ZA Leiden, The Netherlands
[*] Corresponding author: t.e.agbana@tudelft.nl

Compiled May 18, 2017

We have shown that the maximum achievable resolution of in-line lensless holographic microscope is limited by aliasing and, for collimated illumination, can not exceed the camera pixel size. This limit can be achieved only when the optimal conditions on spatial and temporal coherence state of the illumination are satisfied. The expressions defining the configuration, delivering maximum resolution with given spatial and temporal coherence of the illumination are obtained. The validity of these conditions is confirmed experimentally.

OCIS codes: (180.0180) Microscopy, (090.0090) Holography, (030.1640) Coherence.

http://dx.doi.org/10.1364/ao.XX.XXXXXX

Rapid advancement in computational microscopy has opened new possibilities in the design of miniaturized lensless imaging devices and systems with wide applications in biological imaging, especially when simple robust and low-cost solutions are required [1–3]. Lens-less digital in-line holographic microscope (DIHM) represents the simplest possible configuration, as it requires only three components: a light source, sample, and an image sensor [4, 5]. In this system, an object wave interferes with a plane reference wave at the detector plane to form an interferogram as shown in Fig. 1. The complex amplitude of the field in the object plane is numerically reconstructed by solving the inverse source problem, applying back-propagation from the sensor to the sample plane [6, 7]. Unlike the conventional microscope, the instrument can provide details in transparent biological samples since both amplitude and the phase of the field is reconstructed [5, 8–13].

The maximum achievable resolution in lensless in-line holographic microscope is limited by:

- The signal to noise ratio, which depends on the sample size, the diffracted intensity and the detectability of the interference fringes formed at the detector plane [14].
- Spatial aliasing, occurring when the intensity fringes are undersampled by the sensor. Reconstructed images exhibit distortions and fake features, not present in the object.
- Limited spatial and temporal coherence of the source, limiting the maximum observable fringe frequency, limiting the maximum system resolution [15] .

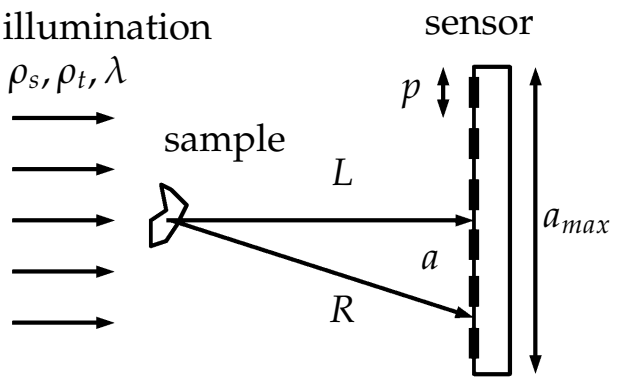

Fig. 1. Schematic of a holographic microscope. The sample is illuminated with a plane wave with wavelength λ, having spatial coherence size of ρ_s and the temporal coherence length of ρ_t. The diffraction pattern is registered by a sensor with pitch p at a distance L .

Noises originating from experimental conditions strengthened by the coherence properties of the illumination source in DIHM has been investigated in [16]. Engineering the optical system geometry with respect to the coherence properties of the source and detector specifications to reduce aliasing has not been considered. This however forms a major difference with our work. Coherence requirement for different holographic setups has been compared by Daniel et-al [15], again this has not been discussed with respect to spatial aliasing.

In this letter we derive the optimal system configuration and illumination properties for achieving the highest possible

resolution with alias-free imaging. Consider a DIHM with the object illuminated by a plane wave with wavelength λ and the coherent properties described by the spatial coherence length ρ_s, and temporal coherence length ρ_t. As shown in Fig 1, the light diffracted by the object interferes with the illumination to form a hologram at the distance L on the detector with pixel pitch p [17, 18].

For alias-free imaging, the minimum period of the fringe pattern, created by the interference between the illumination and the scattered waves, should be at least twice larger than the pitch of the sensor p. To satisfy to this condition, using the notations of Fig. 1, we state:

$$a = \frac{\lambda L}{2p} \tag{1}$$

This relation sets the resolution limit for the microscope. Indeed, since the resolution $r = \lambda/(2A)$ depends on the numerical aperture $A = a/L$, combining these expressions with 1 we obtain the expression for the resolution, as limited by aliasing:

$$r = p. \tag{2}$$

Consider an object with a circular cross section of radius r. As shown by [14, 19], the intensity distribution of the interferogram, obtained with spatially and temporally coherent light, measured at the detector at a distance L from the object is given by:

$$I(a) \approx 1 - \frac{kr^2}{L} \sin\left(\frac{ka^2}{2L}\right) \frac{2\mathrm{J}_1(kar/L)}{(kar/L)} \tag{3}$$

where $k = 2\pi/\lambda$. Using the asymptotic approximation for Bessel function $\mathrm{J}_1(x) \approx \sqrt{\frac{2}{\pi x}} \cos(x - 0.75\pi)$ and neglecting the fast oscillating term $\sin\left(\frac{ka^2}{2L}\right)$, we obtain the expression for the asymptotic envelope of the fringe intensity:

$$I(a)_{env1} \approx 1 - \frac{2}{\pi}\sqrt{\frac{\lambda L r}{a^3}} \cos\left(\frac{kar}{L} - 0.75\pi\right). \tag{4}$$

By neglecting the cos oscillation term in Eq. 4, we obtain the smoothly decaying envelope of the fringe intensity:

$$I_{min} \approx 1 - \frac{2}{\pi}\sqrt{\frac{\lambda L r}{a^3}}; \quad I_{max} \approx 1 + \frac{2}{\pi}\sqrt{\frac{\lambda L r}{a^3}}; \tag{5}$$

Then the fringe visibility as defined in [19, 20], can be estimated with a formula:

$$V(a) = \frac{I_{max} - I_{min}}{I_{max} + I_{min}} \approx \frac{2}{\pi}\sqrt{\frac{\lambda L r}{a^3}}. \tag{6}$$

Since we are interested in the fringe visibility at the edges of our field, the condition of validity of Eq. 6, $\frac{kar}{L} > 1$, is satisfied. Fig. 2 illustrates the fringe intensity calculated for $r = 25$ μm, $L = 0.05$ m and $\lambda = 0.65$ μm according to the exact formula Eq. 3, and using asymptotic approximations 4 and 5.

To avoid aliasing, the fringe visibility should decay to zero at a distance defined by expression 1. In practice, we can consider the fringe to be invisible, when its visibility equals to the inverse of the signal-to noise ratio of the camera:

$$V(a) = S^{-1}. \tag{7}$$

The solution of this equation produces the estimate for the distance providing aliasing-free hologram registration with spatially and temporally coherent illumination:

$$L = \frac{4S}{\pi}\sqrt{\frac{2p^3 r_{max}}{\lambda^2}}. \tag{8}$$

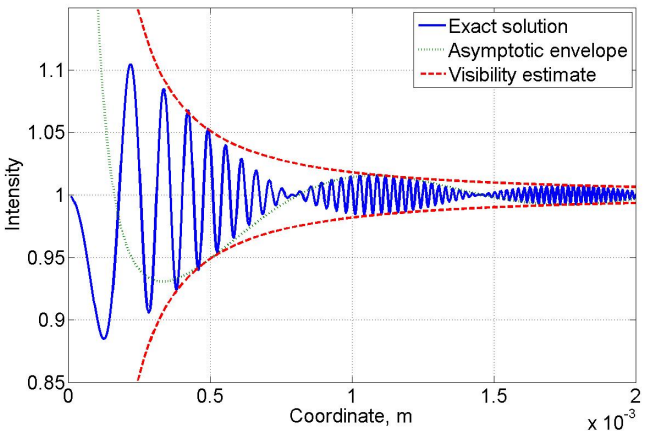

Fig. 2. Fringe intensity calculated for $r = 25$ μm, $L = 0.05$ m and $\lambda = 0.65$ μm according to the exact formula Eq. 3, and using the asymptotic approximations 4 and 5.

According to 6 the fringe visibility is proportional to the square root of the feature size r, therefore, if the object has a range of features, the maximum feature size r_{max} should be used in 8, as then all fringes created by features with $r < r_{max}$ will have lower visibility at $a = \frac{\lambda L}{2p}$. This secures alias-free fringe registration, but causes loss of the fringe patterns created by smaller features, leading to resolution loss.

If the parameters of the sample are unknown, we can require the condition 1 to be satisfied for any place in the sensor, setting the aliasing cutoff size a equal to the sensor size $a = a_{max}$ as shown in Fig. 1, to obtain a condition:

$$L = \frac{2pa_{max}}{\lambda}. \tag{9}$$

If Eq. 9 is satisfied, then the optimal resolution is not achieved for all features of the sample. From the coherent case we can draw conclusions, that will be useful in the further analysis:

- The best achievable resolution of an in-line holographic microscope, limited by aliasing, is in the order of its pixel size. Configuration described by Eq. 9 provides an alias-free compromise with the resolution loss for all feature sizes.
- It is impossible to derive a configuration that provides the optimal fringe visibility for all feature sizes with a coherent illumination. If the smallest feature is optimally resolved without aliasing or loss of fringes due to low visibility, then the larger features will cause aliasing due to higher visibility of high-frequency fringes. If the largest features are imaged free of aliasing, then the smaller features will be imaged with loss of resolution, as the fringe visibility is lost far below the aliasing limit.

So it is of a great interest to control the fringe aliasing by tuning the coherent properties of the illumination. Without any loss of generality, we can assume that, in accordance with the definition of the spatial coherence length ρ_s all fringes with $a > \rho_s$, as shown in Fig. 1, have zero fringe visibility. Then, in the assumption of complete temporal coherence $\rho_t = \infty$, we can define the optimal spatial coherence length for alias-free holographic imaging in the setup shown in Fig. 1:

$$\rho_s = \frac{\lambda L}{2p} \tag{10}$$

This condition provides optimal imaging: larger values of ρ_s result in aliasing, while smaller values cause resolution loss.

Using the Van Cittert-Zernike theorem [21] to express the ρ_s via the numerical aperture of the illumination source A_s and the wavelength: $\rho_s = \lambda/2A_s$, we obtain the expression for the numerical aperture of incoherent illumination, securing alias-free imaging:

$$L = \frac{p}{A_s} \tag{11}$$

For optimal alias-free imaging with extended monochromatic source, the angular size of the camera pixel, as observed from the sample plane, should be equal to the numerical aperture of the illumination source.

In a similar way, in the assumption of absolute spatial coherence $\rho_s = \infty$ of the illumination, expression 1 can be used to derive the limitation to temporal coherence, securing alias-free imaging. The path difference between the illumination and scattered waves should be equal to the coherence length: $R - L = \rho_t$ and accounting for 1 and introducing practical approximation $\rho_t = \frac{\lambda^2}{\Delta\lambda}$ where $\Delta\lambda$ is the illumination linewidth, we solve equation

$$R - L = \sqrt{a^2 + L^2} - L = \frac{\lambda^2}{\Delta\lambda}, \tag{12}$$

to obtain the expression for the illumination linewidth, securing the alias-free registration of interference fringes by the sensor:

$$\Delta\lambda = \lambda^2 \left(\sqrt{\frac{L^2\,(\lambda^2 + 4\,p^2)}{p^2}} - 2\,L \right)^{-1} \approx \frac{4p^2}{L}$$
$$L \approx \frac{4p^2}{\Delta\lambda} \tag{13}$$

where the approximation in the right side of 13 is valid only for $p \gg \lambda$

Expressions 8, 9, 11, 13 define the optimum microscope configuration for different coherence states of illumination. Obviously, these expressions represent rather simplified approximations, derived from physical considerations, that can not replace an in-depth analysis, taking into account the exact distributions of spatio-temporal coherence functions. On the other hand, in practice the coherence functions frequently adhere to simple models, while in more complex practical cases these functions are frequently unknown. Expressions 11 and 13 provide physical insight and guidance for the designing of an optimally-configured instrument, avoiding resolution loss and undersampling.

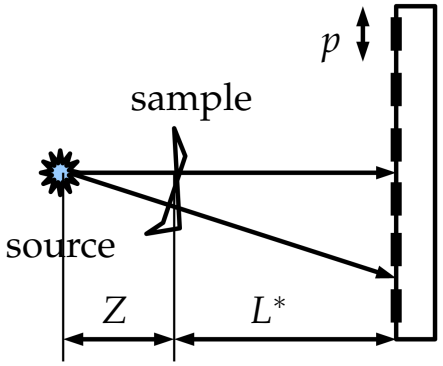

Fig. 3. Microscope configuration with divergent beam, providing sample magnification.

The configuration with diverging illumination, shown in Fig. 3 is of a great practical interest, as it allows to obtain magnified images with magnification $M = \frac{L^*+Z}{Z}$ and resolution $r = p$ in the plane of registration. Configuration with plane wave illumination, shown in Fig. 1 can be made equivalent to the configuration Fig. 3 by satisfying the condition $L = ML^*$:

$$L^* = 0.5(\sqrt{4LZ + Z^2} - Z). \tag{14}$$

Formula 14 is obtained by geometrical analysis, in the paraxial approximation, similar to described in [22]. It is easy to see that $\lim_{Z\to\infty} L^* = L$.

We have conducted a simple experiment, that demonstrates the practical usefulness of the derived models. We designed a microscope using Thorlabs light source S1FC635 Thorlabs with a central wavelenght of 635nm and $\Delta\lambda = 0.8nm$. Since a single-mode fiber was used, a complete spatial coherence and limited temporal coherence was assumed. A commercial CMOS sensor UI-1942LE (3840×2748), with pixel pitch $p = 1.67\mu m$ was used to register the hologram.

We have implemented both configurations: with plane wave, as shown in Fig. 1 and with divergent wave with $Z = 16$ mm, as shown in Fig. 3. Both configurations were tested in three modes: - undersampling, causing strong aliasing, optimal mode described by Eq. 13 and 14, and mode with a too large L, when the high-frequency fringes are lost due to low temporal coherence of the source. The experimental results, shown in Fig. 4, are in good agreement with our expectations, as we have observed undersampling and resolution loss at the expected parameter ranges, with best resolution obtained in a good agreement with our theoretical predictions. Our digital in-line microscope, based on the configuration shown in Fig 3, resolves element 5 of group 7, with feature width of $2.5\mu m$.

The optimized lensless digital microscope has been further tested with biological samples. Schistomsomiasis haematobium eggs $(120 \times 40\mu m)$ in a saline solution prepared on a wet glass slide was imaged using optimized lensless microscope. From the hologram registered by the detector, a high fidelity image showing the eggs with their clearly visible terminal spine was reconstructed as shown in Fig. 5.

In conclusion, we have shown that the maximum achievable resolution of a coherent in-line lensless holographic microscope is limited by aliasing and, for a plane-wave illumination, can not exceed the camera pixel size. Moreover, illumination with coherent light does not allow to achieve optimal aliasing-free imaging for a wide range of feature scales, as the aliasing conditions are significantly different for waves scattered by features with different scales. However, alias-free imaging with resolution equal to the diffraction limit, can be achieved, if we apply special requirements to spatial and temporal coherence of the illumination. The expressions defining the configuration delivering maximum resolution with given coherence state of the illumination are obtained for spatially and temporally incoherent, or partly coherent, light. Matching the microscope parameters to the coherence of illumination is similar to focusing the imaging lens, though the physics and tolerances of these adjustments can not be compared. Experiments, conducted by us, demonstrate clear advantage of instruments, designed with parameters, matched to the coherence of illumination.

T. Agbana's research is supported by TU Delft | Global Initiative, a program of Delft University of Technology to boost Science and Technology for Global Development. The work of H. Gong is sponsored by China Scholarship Council (CSC)

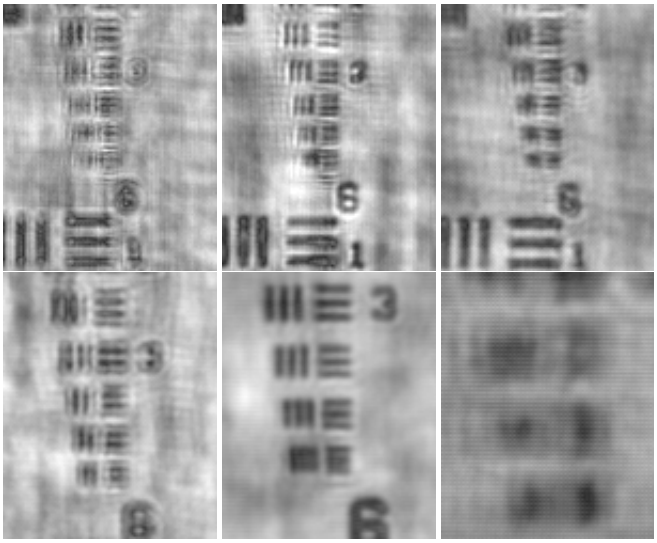

Fig. 4. Test image of group 7 of the USAF resolution chart. Top row registered in the configuration as shown in Fig. 1 with $L = 2$ mm, corresponding to undersampling (left), $L = 13$ mm, corresponding to optimal case described by Eq. 13 (middle), and L=26 mm, corresponding to resolution loss due to low coherence (right). The bottom row is registered in configuration shown in Fig. 3 with $Z = 16$ mm, $L^* = 2$ mm, corresponding to undersampling (left), $L^* = 8.5$ mm, corresponding to optimal case described by Eq. 13 and 14 (middle), and $L^* = 26$ mm, corresponding to resolution loss due to low coherence (right).

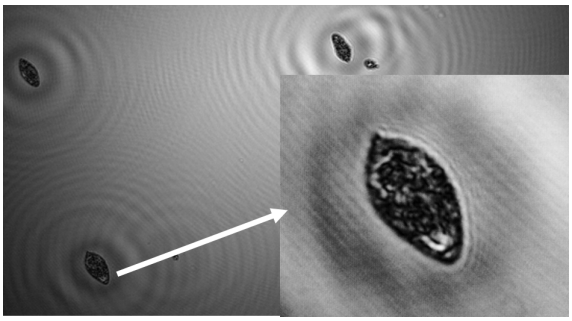

Fig. 5. Reconstructed image of Schistosoma haematobium eggs in a saline solution obtained with optimal configuration of a lensless microscope.

No.201406280043. M. Verhaegen and G. Vdovin are sponsored by the European Research Council (ERC), Advanced Grant Agreement No. 339681. The work of G. Vdovin is partially supported by the program "5 in 100" of the Russian Ministry of Education and Science, and by Flexible Optical BV.

Acknowledgement

The authors acknowledge the support of Prof. Oladimeji Oladepo from University of Ibadan Nigeria, Prof. Maria Yazdanbakhsh, Dr. Chris J. Janse and Dr. Shahid M. Khan from Leiden University, and Dr. O. Soloviev, Dr. P. Pozzi and D. Wilding from TU Delft.

REFERENCES

1. O. Mundanyali, D.Tsend, C.Oh, S.O.Isikman, I.Sencan, W. Bishara, C.Oztoprak, S.Seo, B. Khademhosseini, and A. Ozcan, Lab Chip **10**, 1417 (2010).
2. S.O.Isikman, A.Greenbaum, M.Lee, W. Bishara, O.Mundayali, T.Su, and A. Ozcan, Analytical CellUlar Pathology **35**, 229 (2012).
3. M.Lee, O.Yaglidere, and A.Ozcan, Biomed. Opt.Express **2**, 2721 (2011).
4. A. Ozcan and E.Mcleod, Annu. Rev. Biomed. Eng **18**, 77 (2016).
5. J. B.J.Thompson and W.R.Zinky, Appl. Opt. **6**, 519 (1967).
6. E.Mcleod and A.Ozcan, Rep.Prog.Phys **79** (2016).
7. L.Orzo, Opt. Express **23**, 16638 (2015).
8. D. Gabor, Nature **161**, 777 (1948).
9. W.Xu, M.H.Jericho, I. Meinertzhagen, and H.J.Kreuzer, PNAS **98**, 11601 (2001).
10. E.Serabyn, K.Liewer, C.Lindensmith, K. Wallace, and J.Nadeau, Opt. Express **24**, 28540 (2016).
11. U. Schnars and W. P. Juptner, Measurement Science and Technology **13**, R85 (2002).
12. C. M.Kanka, A.Wuttig and R.Riesenberg, Opt.Lett. **35**, 217 (2010).
13. M. H. J.Garcia-Sucerquia, Wenbo Xu, Opt.Lett. **31**, 1211 (2006).
14. P. Dunn and B.J.Thompson, Optical Engineering **21**, 327 (1982).
15. D.Claus, D.Iliescu, and J.M.Rodenburg, Appl.Opt. **52**, A326 (2013).
16. J. Garcia-Sucerquia, Appl.Opt. **52**.
17. U. Schnars and W. Jueptner, *Digital Holography: Digital Hologram Recording, Numerical Reconstruction and Related Techniques* (Springer, 20051957).
18. V. de Hulst H.C, *Light scattering by small particles* (John Wiley and Sons, 1957).
19. G.A.Tyler and B.J.Thompson, Optica Acta: International Journal of Optics **23**, 685 (1976).
20. F. Pedrotti, Leno.M.Pedrotti, and Leno.s.Pedrotti, *Introduction to Optics* (Pearson Education Limited, 2002).
21. M.Born and E.Wolf, *Principle of Optics, 7th ed.* (Cambridge University, 2002).
22. E. A. Sziklas and A. E. Siegman, Appl. Opt. **14**, 1874 (1975).

FULL REFERENCES

1. O. Mundanyali, D.Tsend, C.Oh, S.O.Isikman, I.Sencan, W. Bishara, C.Oztoprak, S.Seo, B. Khademhosseini, and A. Ozcan, "Compact, light-weight and cost-effective microscope based on lensless incoherent holography for telemedicine applications," Lab Chip **10**, 1417–1428 (2010).
2. S.O.Isikman, A.Greenbaum, M.Lee, W. Bishara, O.Mundayali, T.Su, and A. Ozcan, "Lensfree computational microscopy tools for cell and tissue imaging at the pont-of-care and in low-resource settings," Analytical CellUlar Pathology **35**, 229–247 (2012).
3. M.Lee, O.Yaglidere, and A.Ozcan, "Field-portable reflection and transmission microscopy based on lensless holography," Biomed. Opt.Express **2**, 2721–2730 (2011).
4. A. Ozcan and E.Mcleod, "Lensless imaging and sensing," Annu. Rev. Biomed. Eng **18**, 77–102 (2016).
5. J. B.J.Thompson and W.R.Zinky, "Application of hologram techniques for particle size analysis," Appl. Opt. **6**, 519–526 (1967).
6. E.Mcleod and A.Ozcan, "Unconventional methods of imaging: computational microscopy and compact implementations," Rep.Prog.Phys **79** (2016).
7. L.Orzo, "High speed phase retrieval of in-line holograms by the aassistance of corresponding off-axis holograms," Opt. Express **23**, 16638–16649 (2015).
8. D. Gabor, "A new microscopiic principle," Nature **161**, 777–778 (1948).
9. W.Xu, H.Jericho, I.Meinertzhagen, and D.Kreuzer, "Digital in-line holography for biological applications," PNAS **98**, 11601–11305 (2001).
10. E.Serabyn, K.Liewer, C.Lindensmith, K. Wallace, and J.Nadeau, "Compact, lensless digital holographic microscope for remote microbiology," Opt. Express **24**, 28540–28548 (2016).
11. U. Schnars and W. P. Juptner, "Digital recording and numerical reconstruction of holograms," Measurement Science and Technology **13**, R85 (2002).
12. C. M.Kanka, A.Wuttig and R.Riesenberg, "Fast exact scalar propagation for an in-line holographic microscopy on the diffraction limit," Opt.Lett. **35**, 217–219 (2010).
13. M. H. J.Garcia-Sucerquia, Wenbo Xu, "Immersion digital in-line holographic microscopy," Opt.Lett. **31**, 1211–1243 (2006).
14. P. Dunn and B.J.Thompson, "Object shape, fringe visibility and resolution in far-field holography," Optical Engineering **21**, 327–332 (1982).
15. D.Claus, D.Iliescu, and J.M.Rodenburg, "Coherence requirement in digital holography," Appl.Opt. **52**, A326–A335 (2013).
16. J. Garcia-Sucerquia, "Noise reduction in digital lensless holographic microscopy by engineering the light from a light-emitting diode," Appl.Opt. **52**.
17. U. Schnars and W. Jueptner, *Digital Holography: Digital Hologram Recording, Numerical Reconstruction and Related Techniques* (Springer, 20051957).
18. V. de Hulst H.C, *Light scattering by small particles* (John Wiley and Sons, 1957).
19. G.A.Tyler and B.J.Thompson, "Fraunhofer holography applied to particle size analysis a reassessment," Optica Acta: International Journal of Optics **23**, 685–700 (1976).
20. F. Pedrotti, Leno.M.Pedrotti, and Leno.s.Pedrotti, *Introduction to Optics* (Pearson Education Limited, 2002).
21. M.Born and E.Wolf, *Principle of Optics, 7th ed.* (Cambridge University, 2002).
22. E. A. Sziklas and A. E. Siegman, "Mode calculations in unstable resonators with flowing saturable gain. 2: Fast fourier transform method," Appl. Opt. **14**, 1874–1889 (1975).